

## Analysis of Changes in Strain State Induced by Hydrocarbon Production in Onshore Fuba Field Niger Delta, Nigeria, Using 3-D Seismic Time-lapse Data

U. Ochoma<sup>1\*</sup>

<sup>1</sup>Department of Physics, Rivers State University, P.M.B. 5080, Port Harcourt, Nigeria.  
Corresponding Author (U. Ochoma) Email: umaocho@gmail.com\*



DOI: Under Assignment

Copyright © 2026 U. Ochoma. This is an open-access article distributed under the terms of the Creative Commons Attribution License, which permits unrestricted use, distribution, and reproduction in any medium, provided the original author and source are credited.

Article Received: 21 February 2026

Article Accepted: 23 April 2026

Article Published: 25 April 2026

### ABSTRACT

Analysis of changes in strain state induced by hydrocarbon production in Onshore Fuba Field Niger Delta, Nigeria, are here presented, using 3D seismic time-lapse data. The base (1997) and the monitor (2009) seismic surveys resulted in a 4D response difference. The Base and Monitor data have an RRR (root-mean-square repeatability ratio) of 0.38 implying a very good repeatability when considering the acquisition, processing and environmental noises. Data processing and interpretation were carried out using Petrel software. Reservoir pressure decline rate of 0.062 psi/day resulted in production decline rate of 1192.21 bbl/day. Structural interpretation of seismic data reveals a highly faulted field. Two distinct horizons were mapped. Fault and horizon interpretation shows closures that are collapsed crestal structures bounded by two major faults. Reservoirs are found at a shallower depth from 10937 to 10997 ft and at a deeper depth ranging from 11681 to 11871 ft. The variance edge and chaos enhanced the faults or sedimentological bodies within the seismic data volume. There are more discontinuities in the difference volume variance edge and chaos which show that there is production-induced fracturing in the field of study. The lengths, dips and orientations of the faults and horizons, in the base and monitor stacks, are not equal indicative of production-induced fault re-activation. The difference volume acoustic impedance shows the lowest relative acoustic impedance indicating reduced porosity and permeability due to hydrocarbon production while the difference volume sweetness shows reduced high-amplitude areas due to hydrocarbon production. The results of the work can be applied in the hydrocarbon exploitation scheme to minimize the damages associated with production and to ascertain reactivation of faults in the area of study.

**Keywords:** Hydrocarbon; Base; Monitor; Difference Volume; Seismic; Time-Lapse; Faults; Variance Edge; Sweetness; Niger Delta; Nigeria.

### 1. Introduction

Time-lapse seismic monitoring of production-induced changes in a reservoir and the surrounding rocks over time has the basic aim of mapping reservoir compartments and subsurface rock deformation, monitoring fluid movement and pore pressure changes, identifying by-passed oil and planning for future production performance, and this has been challenging (Calvert et al., 2018; Stammeeijer, and Hatchell, 2014; Herwanger and Koutsabeloulis, 2011; Landrø, 2001; Trani, et al., 2011; MacBeth, et al., 2018). Pore pressure depletion creates changes in the stress and strain fields of the rock material both inside and outside the reservoir (Prioul, et al., 2004; Fuck, et al., 2011; Ochoma, 2024). In addition to leakage of hydrocarbons, hazards are associated with wells crossing reactivated faults (Alsos, et al. 2002). Compaction causes reduction in porosity and permeability which affect production. Porosity loss affects the computation of oil and gas reserves (Pourciau et al., 2005).

This study is taken from Fuba Field, Depobelt, Niger Delta, Nigeria. The ultimate deliverable of this study was analysis of changes in strain state induced by hydrocarbon production using 3-D seismic time-lapse data. The major components of this study are: (a) Well Correlation performed in order to determine the continuity of the reservoir sand across the field. (b) Seismic Interpretation which involves differencing of seismic volume, well-to-seismic tie, fault mapping, horizon mapping, time surface generation, depth conversion and seismic attributes generation. This aids in giving more insight into analysis of changes in strain state induced by hydrocarbon production in onshore Fuba field Niger Delta, Nigeria, using 3-D seismic time-lapse data.

The proposed study area Fuba Field is located in the onshore Niger Delta region. Figure 1 shows the map of the Niger Delta region showing the location of the study area and the base map showing well locations in the study area. The Niger Delta lies between latitudes 4° N and 6° N and longitudes 3° E and 9° E (Whiteman, 1982). The Delta ranks as one of the major oil and gas provinces globally, with an estimated ultimate recovery of 40 billion barrels of oil and 40 trillion cubic feet of gas (Adegoke, et al., 2017). The coastal sedimentary basin of Nigeria has been the scene of three depositional cycles (Short, and Stauble, 1967). The first began with a marine incursion in the middle Cretaceous and was terminated by a mild folding phase in Santonian time. The second included the growth of a proto-Niger delta during the Late Cretaceous and ended in a major Paleocene marine transgression. The third cycle, from Eocene to Recent, marked the continuous growth of the main Niger delta. A new threefold lithostratigraphic subdivision is introduced for the Niger delta subsurface, comprising an upper sandy Benin Formation, an intervening unit of alternating sandstone and shale named the Agbada Formation, and a lower shaly Akata Formation. These three units extend across the whole delta and each range in age from early Tertiary to Recent. They are related to the present outcrops and environments of deposition. A separate member of the Benin Formation is recognized in the Port Harcourt area. It is Miocene-Recent in age with a minimum thickness of more than 6,000 ft (1829 m) and made up of continental sands and sandstones (>90 %) with few shale intercalations (Horsfall, et al., 2017). Subsurface structures are described as resulting from movement under the influence of gravity and their distribution is related to growth stages of the delta (Ochoma, 2024). Rollover anticlines in front of growth faults form the main objectives of oil exploration, the hydrocarbons being found in sandstone reservoirs of the Agbada Formation. The oil in geological structures in the basin may be trapped in dip closures or against a synthetic or antithetic fault.

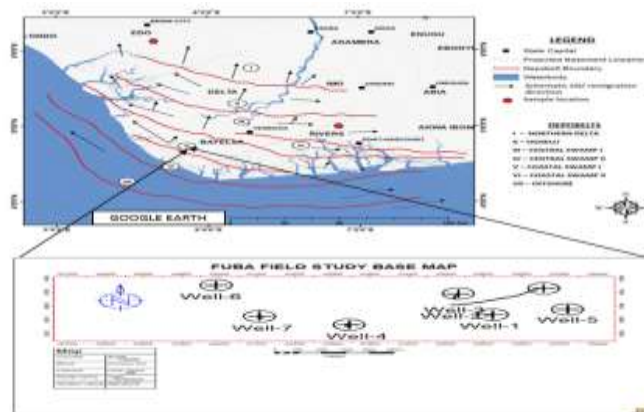


**Figure 1.** Map of Niger Delta Showing the Study Area

(Source: Google Earth 2026) and Base Map Showing Well Locations in the Study Area

### 1.1. Study Objectives

The objectives of the study include the following:

- 1) Generation of difference cube from the base and monitor data and quantification of the RRR (repeatability) for the time-lapse data.
- 2) Delineation of reservoir units.

- 3) Generation of synthetic seismogram and well-to-seismic tie.
- 4) Generation of time surfaces.
- 5) Generation of seismic attributes.
- 6) Converting reservoir surfaces from time to depth.

## 2. Literature Review

Many literatures have reported interesting seismic time-lapse studies in the oil prolific area of the Niger Delta Basin, Nigeria. Furthermost, these studies majored on time-lapse feasibility studies and reservoir monitoring and management (Aniwetalu, et al., 2017). Moreover, literatures in public domain are very scarce on seismic time-lapse, in Nigeria, with the main objective of determining effect of hydrocarbon production on subsurface structures and faults reactivation (Igwenagu, et al, 2021). Ochoma, (2023) found that there are more discontinuities in the difference volume variance edge which implies that there are more cracks in the field of study due to production. The lengths, dips and orientations of the faults and horizons, in the base and monitor stacks, are not equal indicative of faults reactivation that could have resulted from hydrocarbon production. Ogbamikhumi et al., (2017) evaluated the effect of changes in reservoir fluid saturations on time-lapse seismic amplitudes. Rock physics modelling and fluid substitution studies on well logs were carried out, and acoustic impedance change in the reservoir was estimated to be in the range of 0.25 % to about 8 %. Changes in reservoir fluid saturation were confirmed with time-lapse amplitudes within the crest area of the reservoir structure where porosity is 0.25 %. They demonstrated the use of repeat seismic to delineate swept zones and areas hit with water override in a producing onshore reservoir.

Liang, et al., (2025) used field measurements and an analysis of surface subsidence data from high-intensity longwall mining operations at the Xiaobaodang Number 2 Coal mine for revealing characteristic ground movement patterns under intensive extraction conditions. The subsidence basin was systematically divided into pipeline hazard zones using three key deformation indicators: horizontal strain, tilt, and curvature. Through abaqus-based 3D numerical modeling of coupled pipeline–coal seam mining systems, this research elucidated the spatiotemporal evolution of pipeline Von Mises stress under varying mining parameters, including working face advance rates, mining thicknesses and pipeline orientation angles relative to the advance direction. The simulations further uncovered non-synchronous deformation behavior between the pipeline and its surrounding sand and soil, identifying two distinct evolutionary phases and three characteristic response patterns. Based on these findings, targeted pipeline integrity preservation measures were developed, with numerical validation demonstrating that maintaining advance rates below 10 mD, restricting mining heights to under 2.5 m within the 260 m pre-mining influence zone, and where geotechnically feasible, the maximum stress of the pipeline laid perpendicular to the propulsion direction (90°) can be controlled below 480 MPa, and the separation amount between the pipe and the sand and soil can be controlled below 8.69 mm, which can effectively reduce the interference caused by mining. These results provide significant engineering guidance for optimizing longwall mining parameters while ensuring the structural integrity of shallow-buried pipelines in high-intensity extraction environments.

Karanam, and Lu, (2025) used poroelastic modeling and InSAR (Interferometric Synthetic Aperture Radar) to investigate the role of geology and subsurface pressure changes in surface deformation within the Delaware Basin, the most productive sub-basin of the Permian Basin. First, sentinel-1 SAR data were processed using persistent scatterer interferometry (PSI) techniques to obtain surface deformation time series. The results indicate that a large portion of the Delaware Basin is subsiding, with two prominent deformation hotspots to the north of the Grisham Fault Zone (GFZ), subsiding at a rate of 3-4 cm/yr. Then, focusing on the Northern Delaware Basin, where seismicity is minimal and subsidence primarily exhibits radial patterns, they developed a fully coupled poroelastic model in COMSOL® Multiphysics that integrates the conservation of momentum and mass to simulate subsurface fluid behavior. The model incorporates well data, fluid injection/extraction volumes, fault layers, and geological stratigraphy to simulate stress and pore pressure changes from hydrocarbon extraction and wastewater injection. Faults were modeled as discrete elements that either block or facilitate fluid movement, depending on their orientation and permeability. The results highlight the complex relationship between hydrocarbon production, waste water injection, subsurface geology, fluid pressure propagation and surface deformation. The model's predictions were then validated using InSAR-derived surface deformation data, offering a detailed understanding of stress and strain dynamics in the region. This study provides valuable insights into subsurface deformation in hydrocarbon-producing regions, with potential applications for assessing risks to infrastructure, seismicity and environmental health.

### 3. Methodology

#### 3.1. NRMS (Normalized Root Mean Square) Repeatability (RRR) and Differencing of Seismic Volume

Pre-stack time migrated full-offset base and monitor stacks were available. The success of time-lapse reservoir monitoring depends on removing the non-repeatable effects such as configurations, seasonal changes, atmospheric temperatures, tides, elastic properties of the overburden, compaction, multiples, and rock heterogeneities (Vedanti, et al., 2009; Varela, et al., 2006). Obstructions, weather patterns, cost constraints, and maritime traffic can also influence the survey orientation. Having considered the above sources of error in repeatability, the acquisition system itself, positioning accuracy, receiver sensitivity/calibration, and source calibration must also be looked into. All these sources of error were handled through normalized root mean square (NRMS) analysis. The NRMS value is simply the RMS amplitude of the difference, normalized by the average of the RMS amplitudes of the baseline data Baseline and monitor data Monitor (Kragh, and Christie, 2002):

$$NRMS = \frac{2 \text{rms}(\text{Monitor} - \text{baseline})}{\text{rms}(\text{Monitor}) + (\text{Baseline})} \quad (1)$$

$$\text{rms} = \sqrt{\frac{\sum x_i^2}{N}} \quad (2)$$

The summation is over N number of all samples  $x_i$  ( $i = 1, 2, \dots, N$ ) in the time window.

The NRMS value is a measure of non-repeatability. If NRMS = 0, the data are perfectly repeatable. Typical “good” values of NRMS quoted in the literature range from 0.1 to 0.3 [10 % to 30 % non-repeatability] (Johnston, 2013).

Monitor seismic volume was subtracted from the base seismic volume and the differences was interpreted to determine the areas of the field that have been changed during production. Areas of the field where there have been changes were analyzed and compared to production activity in those areas.

### 3.2. Well-to-Seismic Ties

Well correlation is the first stage of the pre-interpretation process. The process of well correlation involves lithologic description, picking top and base of sand-bodies, fluid discrimination and then linking these properties from one well to another based on similarity in trends. In between these two lithologies in the subsurface, the gamma ray log is often used. Correlation of reservoir sands was achieved using the top and base of reservoir sands picked. The correlation process was possible based on similarity in the behaviour of the gamma ray log the Niger Delta; the predominant lithologies are sands and shales. In order to discriminate shapes. Also, the thickness of the shale bodies overlying and underlying the sand body is considered during Correlation. After defining the lithologies, the resistivity log was used for discriminating the type of fluid occurring within the pores in the rocks. There are seven basic steps involved in seismic interpretation relevant to this study and they include; Differencing of seismic volume, Well-to-seismic ties, Fault mapping, Horizon mapping, Time surface generation, Depth conversion and Seismic attributes generation. Well-to-seismic tie is a process that enables the visualization of well information on seismic data. For this process to be achieved, the following are basic requirements; checkshot, sonic log, density log and a wavelet. The sonic log, which is the reciprocal of velocity, was calibrated using the checkshot data. The calibration process is necessary in order to improve the quality of the sonic log because the sonic log is prone to washouts and other wellbore related issues. The results of calibrating the sonic log with the checkshot gives a new log called the calibrated sonic log.

The calibrated sonic log is used along with the density log to generate an acoustic impedance (AI) log. The acoustic impedance log is calculated for each layer of rock. The next step involves generating the RC (reflectivity coefficient) log. The RC is calculated and generated using the AI log. The RC log generated is then convolved with a wavelet to generate a synthetic seismogram which is comparable with the seismic data. The statistical wavelet utilized for convolution is extracted from the seismic data. The synthetic seismogram was generated for every well that had checkshot, density and sonic log. The reflections on the synthetic seismogram were matched with the reflections on seismic data. The mathematical expressions that govern the entire well-to-seismic tie workflow are presented below;

$$AI = \rho v \quad (3)$$

$$RC = \frac{\rho_2 v_2 - \rho_1 v_1}{\rho_2 v_2 + \rho_1 v_1} \quad (4)$$

$$\text{Synthetic Seismogram} = \frac{\rho_2 v_2 - \rho_1 v_1}{\rho_2 v_2 + \rho_1 v_1} * \text{wavelet} \quad (5)$$

Where  $\rho$  = Density,  $v$  = Velocity, AI = Acoustic impedance and RC = Reflection coefficient.

Faults were identified as discontinuities or breaks in the seismic reflections. Faults were mapped on both inline and cross-line directions. Horizons are continuous lateral reflection events that are truncated by fault lines. The horizon interpretation process was conducted along both inline and crossline direction. At the end of the horizon mapping,

a seed grid is generated which serves as an input for time surface generation. Time surfaces were generated using the seed grids gotten from the horizon mapping process. The third order polynomial velocity model was generated and used to depth convert the time surfaces of the reservoirs of interest.

### 3.3. Dip magnitude

Dip magnitude is analogous to strike and dip of sedimentary layers. The dip magnitude is defined as the angle between the steepest direction of a plane and a horizontal plane, where values range from 0 to 90. The dip magnitude attribute computation in Petrel software makes use of the inbuilt formula:

$$\text{True dip} = \tan^{-1}\left(\frac{\tan(\theta_y)}{\tan(\beta_x)}\right) \quad (6)$$

where  $\theta_y$  = apparent dip in a direction (y) and  $\beta_x$  = dip azimuth relative to a direction (x).

Dip magnitude is a good attribute not only for showing overall structure folds, but can be used to identify faults with very small displacement.

### 3.4. Variance (Edge Detection) Method

The variance attribute is edge imaging and detection techniques. It is used for imaging discontinuity related to faulting or stratigraphy in seismic data. Variance attribute is proven to help in imaging of channels, fault zones, fractures, unconformities and the major sequence boundaries. In the Petrel software, the variance attribute uses an algorithm that computes the local variance of the seismic data through a multi-trace window with user-defined size. The local variance is computed from horizontal sub-slices for each voxel. A vertical window was used for smoothing the computed variance and the observed amplitude normalized. The variance attribute measures the horizontal continuity of the amplitude that is the amplitude difference of the individual traces from their mean value within a gliding CMP window.

$$\sigma^2 = \frac{1}{n} \sum_{f_i=1}^n (x_i - x_m)^2 \quad (7)$$

Where  $\sigma$  = standard deviation,  $\sigma^2$  = variance,  $n$  = the number of observations,  $f_i$  = frequency

$x_i$  = the variable and  $x_m$  = mean of  $x_i$ .

### 3.5. Chaos

Chaos attribute is defined as a measure of the “lack of organization” in the dip and azimuth estimation method. It can be used to distinguish different sediment facies in lithology variation environments (for example, sand and shale).

### 3.6. Determination of Relative Acoustic Impedance

The acoustic impedance inversion transforms the seismic data into an acoustic impedance model. The acoustic impedance of a media is given as

$$AI = \rho v \quad (8)$$

where AI = acoustic impedance,  $\rho$  = density,  $v$  = velocity.

To measure acoustic impedance, it is necessary to use seismic inversion. It was assumed that the input seismic data has been processed to reduced noise and multiples, and also contains zero phase and large bandwidth. The seismic trace represents a band-limited reflective series;

$$f(t) = \frac{1}{2} \frac{\Delta \rho v}{\rho v} \quad (9)$$

where  $f(t)$  = seismic trace,  $\Delta \rho v$  = the difference in the product of density and velocity. The integration of the seismic trace will provide a bandlimited estimate of the natural log of the acoustic impedance. Since the integration of band-limited, the impedance will not have absolute magnitude values and consequently is only relative. Relative acoustic impedance is an estimated inversion computed by the integration of seismic trace accompanied by a high cut Butterworth zero-phase filter. It is a simplified inversion and has been generated as an asynchronous attribute in the software. It enhances acoustic impedance contrast boundaries. According to Schlumberger's (2007a), the relative acoustic impedance (RAI) can be computed by integrating the real part of the seismic trace.

$$\ln(\rho v) = 2 \int_{t=0}^{t=1} f(T) dt \quad (10)$$

Where  $f(T)$  = real part of seismic trace. A Butterworth filter is then applied to remove long-wavelength trends that originated from the integration process (Taner, 2001).

$$BL(f) = \frac{1}{1 + \left(\frac{f}{f_H}\right)^{2N}} \quad (11)$$

where  $BL(f)$  = band-limited signal in frequency;  $f_H$  = frequency cut-off value of 10 Hz,  $N$  = filter order of 3.

It is used for delineating sequence boundaries, unconformity surfaces, and discontinuities. The acoustic impedance may be related to the formation porosity and the presence of fluid in a hydrocarbon reservoir.

### 3.7. Determination of Sweetness

Sweetness involves the implementation of envelopes and instantaneous frequency that are combined. Mathematically, it is expressed as

$$S(t) = \frac{\alpha(t)}{\sqrt{f_\alpha(t)}} \quad (12)$$

where  $S(t)$  = Sweetness,  $\alpha(t)$  = Envelope,  $f_\alpha(t)$  = instantaneous frequency.

Sweetness is used for the identification of features where the total energy signatures change in the seismic data.

## 4. Results and Discussion

### 4.1. Production Data

The production and reservoir pressure reports are presented in Figures 2 and 3. Production decline of 1192.21 bbl/day resulted from pressure decline of 95.50 bar/year or 0.062 psi/year.

#### 4.2. Normalized Root Mean Square (NRMS) Repeatability (RRR) and 4D Response

The NRMS of 0.38 has been achieved, in this study, implying very good repeatability when considering the quality of data and acquisition difference. The seismic time-lapse difference between the base and monitor surveys was successfully extracted. The fact of the difference from the monitor implies the existence of production-induced effect and acquisition, environmental and processing noises, hence the 4D or time-lapse response signal.

#### 4.3. Reservoir Identification, Correlation and Well-to-Seismic Ties

The results for lithology and reservoir identification are presented in Figure 4. A total of four sand bodies (L, M, N and O) were identified and correlated across all seven wells in the field. Two reservoir sands were selected for the purpose of this study (Reservoirs M and O). The resistivity logs which reveals the presence of hydrocarbons were used to identify the hydrocarbon bearing sands. On Figure 4, the sands are coloured yellow while shales are grey in colour. The results for well-to-seismic tie conducted on Fuba field using density log, sonic log and checkshot of Well-1 is presented in Figure 5. Extended white 2 wavelet was used to give a near perfect match between the seismic and synthetic seismogram.

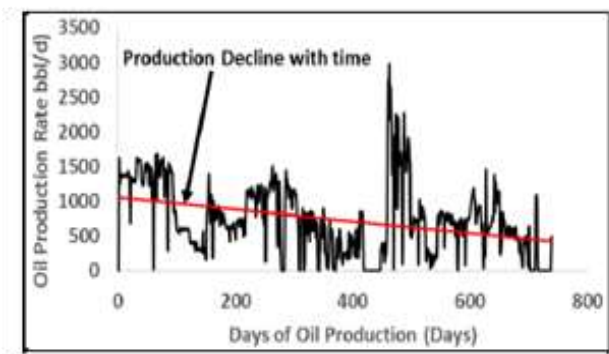


**Figure 2.** Reservoir Production Rate versus Days of Oil Production, Showing the Decline in Production Rate over Time.

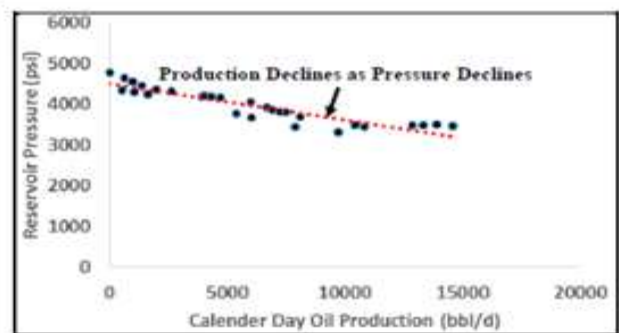


**Figure 3.** Effect of Reservoir Pressure Decline (95.50 bar/year or 0.062 psi/year) on Oil Production Performance.

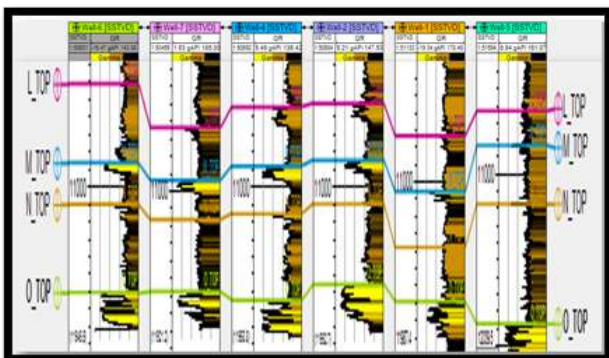


**Figure 4.** Well Section Showing Reservoirs L, M, N, and O Identified and Correlated Across the Fuba Field.

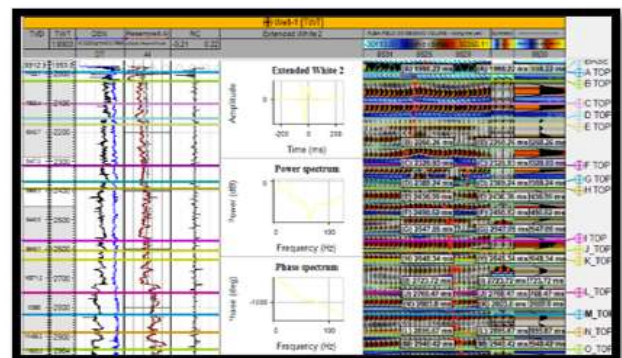


**Figure 5.** Synthetic Seismogram Generation and Well-to-Seismic Tie for the Fuba Field Using Well-1 Checkshot Data.

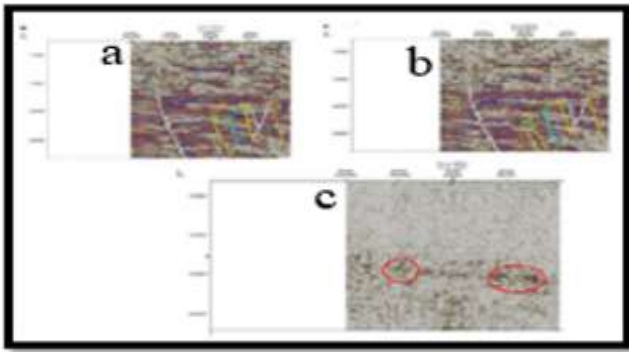


**Figure 6.** Base, Monitor, and Difference Seismic Sections for Inline 8590 Showing the Interpreted Fault Framework.

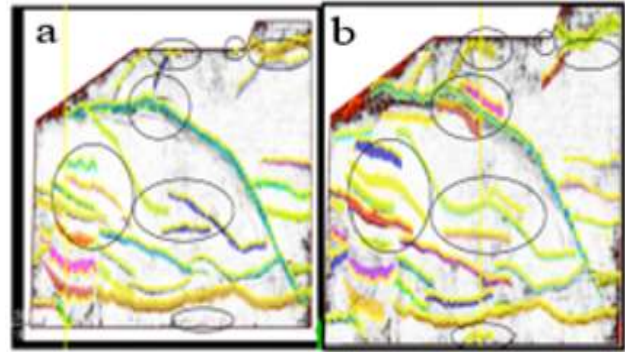


**Figure 7.** 4D Seismic Difference Response Between Base and Monitor Surveys, with Interpreted Faults Displayed on the Variance Time Slice at Z = 2060 ms.

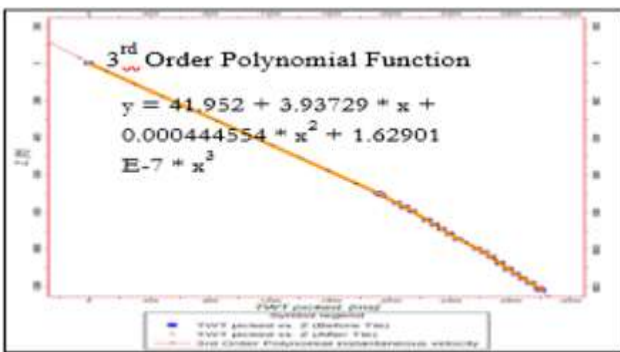


**Figure 8.** Third-Order Polynomial Velocity Model Used for Converting Reservoir Horizons from Time to Depth Domain.

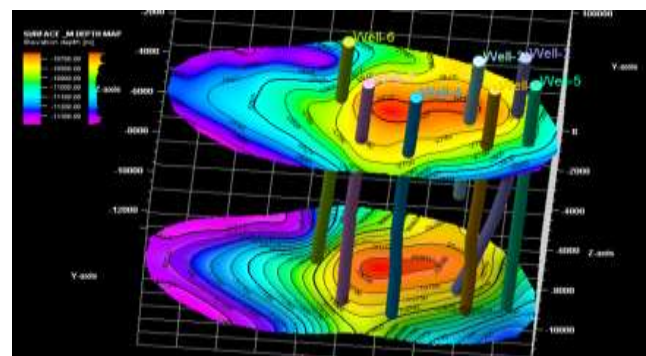


**Figure 9.** Depth Structure Map of Reservoir M Showing an Anticlinal Closure Supported by Faulting.

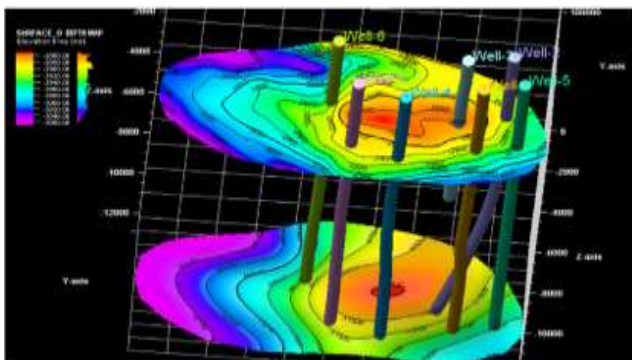


**Figure 10.** Depth Structure Map of Reservoir O Showing an Anticlinal Closure Supported by Faulting.

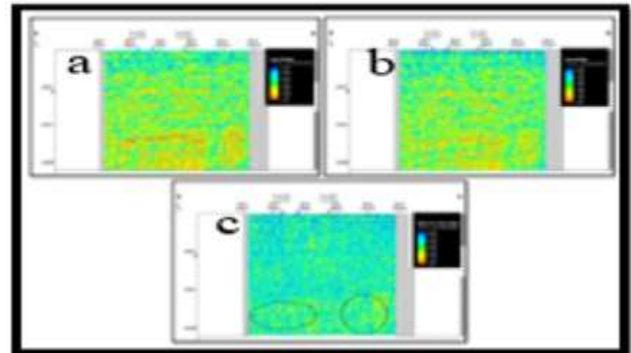


**Figure 11.** Dip Magnitude Along Inline 8515 Showing Production-Induced Fault Reactivation.

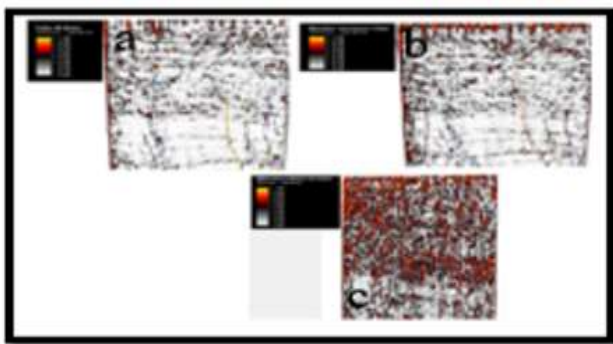


**Figure 12.** Variance Edge Along Inline 8515 Showing Production-Induced Fracturing.

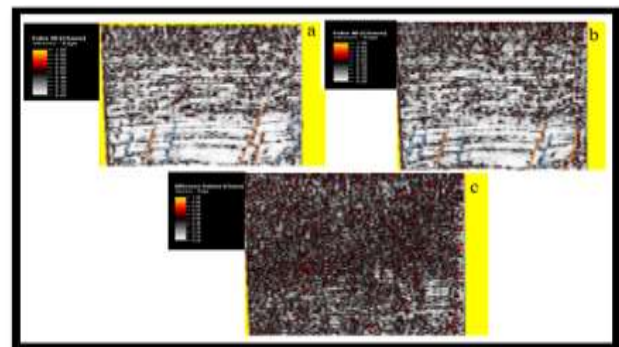


**Figure 13.** Chaos Attribute Along Inline 8515 Showing Production-Induced Fracturing.

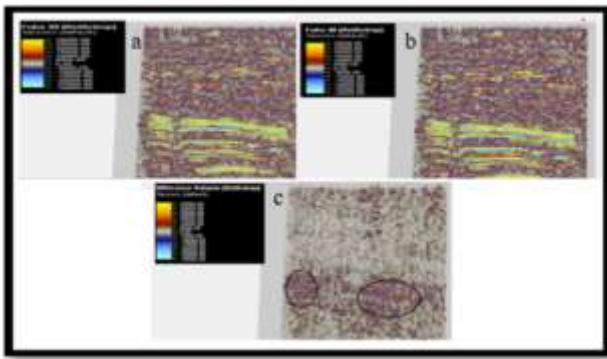


**Figure 14.** Acoustic Impedance Along Inline 8515 for the Base, Monitor, and Difference Volumes, Indicating Reduced Porosity and Permeability Due to Hydrocarbon Production.

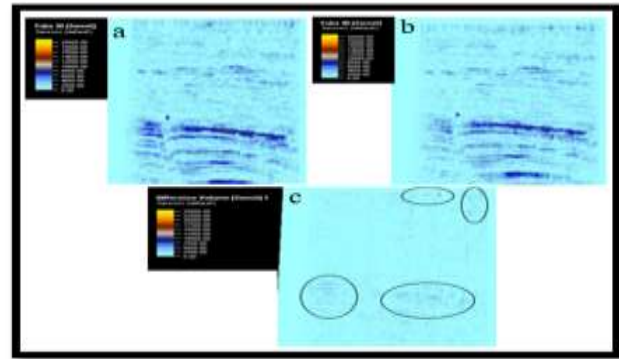


**Figure 15.** Sweetness Attribute Along Inline 8515 for the Base, Monitor, and Difference Volumes, Showing Reduced High-Amplitude Areas Due to Hydrocarbon Production.

#### 4.4. Fault and Horizon Interpretation

The results for the interpreted faults in Fuba field are presented in Figure 6 shows both synthetic and antithetic faults interpreted along seismic inlines. Faults are more visible along the inline direction because this direction reveals the true dip position of geologic structures. The variance time slice at  $Z=2060$  was used to validate the interpreted faults as shown in Figure 7. The areas in black circles indicate the 4D response. All interpreted faults are normal synthetic and antithetic faults. A total of thirty-six faults were interpreted across the entire base seismic data while forty faults were interpreted across the entire monitor seismic data. There is depletion of hydrostatic pressure due to production. So, areas that were cracks or fissures on the base seismic became relaxed and became well-defined or pronounced faults on the monitor seismic. There are more faults on the monitor seismic than the base seismic. It also indicates that some of these faults are of higher extents and more pronounced on the monitor seismic. Of the interpreted faults, only F1 (synthetic fault) and F16 (antithetic fault) faults are regional, running from the top to bottom across the field. Hence, these faults play significant roles in trap formation at the upper, middle and lower sections of the field. In Fuba Field, the lengths, dips and orientations of faults are not equal in both base and monitor seismic sections suggestive of fault reactivation from hydrocarbon production. The results for the interpreted seismic horizons (Horizons M and O) are also presented in Figure 6. On these horizons, the fault polygons were generated and eliminated. The horizons were used as inputs for the generation of reservoir time surfaces. The reservoir time surfaces (M and O reservoirs) reveal that the reservoir structure is a collapsed crest, bounded by two regional faults (F1 and F16). Figure 8 shows the 3<sup>rd</sup> order polynomial velocity model which was selected and used as most suitable velocity model for converting M and O reservoirs from time to depth. The depth converted reservoir M and O surfaces are presented in Figures 9 and 10 for the third order polynomial velocity function. The depth structure maps indicate that the reservoirs are anticlinal and fault supported. Reservoir M is found at a shallower depth from 10937 to 10997 ft while reservoir O is found at a deeper depth ranging from 11681 to 11871 ft.

#### 4.5. Seismic Attributes

Figure 11 shows the dip magnitude of the faults for the base, monitor and difference volume. The dip magnitude values range from 0 to 90 degrees. On Figure 11, the green colors represent areas of greater dip, while the red

colors represent areas of shallower dip. The dip magnitude of the faults is not equal as indicated by the difference volume (Figure 11c). This shows that there is production-induced fault re-activation in Fuba field.

Figures 12 and 13 show the computed variance attributes and chaos of the seismic section. The variance and chaos values range from 0.0 to 1.0. Values of variance equal to 1 represent discontinuities while a continuous seismic event is represented by the value of 0. The high values are denoted with red to yellow colorations. There are more discontinuities in Figures 12c and 13c which show that there is production-induced fracturing in the field of study.

Concerning the variance map, the areas dotted with blue, green, orange and pink colored lines signify values that correspond to the location of the discontinuity. The discontinuities may be interpreted as faults and boundaries as shown by the lines drawn on the variance attribute map (Law, and Chung, 2006). The variance edge enhanced the faults or sedimentological bodies within the seismic data volume. Furthermore, several bright spots are also delineated (in black circles and black ovals) which indicate high reflectivity sediments compared to their surroundings. These bright spots are an indication that a potential hydrocarbon trap might exist in the area. The variance attribute is edge imaging and detection techniques. It is used for imaging discontinuity related to faulting or stratigraphy in seismic data. Variance attribute is proven to help in imaging of channels, fault zones, fractures, unconformities and the major sequence boundaries (Pigott, et al., 2013). The darkest regions in the seismic section, which make vertical strips, may be interpreted as faults or fractures. The zones with low variance values are due to similar seismic traces. Areas with red patches represent lineaments/discontinuities while grey areas represent the structural framework of the field.

The relative acoustic impedance generated in the study area is shown in Figure 14. Based on the map, the yellow and red colours represent the highest relative impedance (in black circles) while the lowest relative impedance is represented by the blue colour.

The relative acoustic impedance attribute represents apparent acoustic impedance or physical property contrasts. It is commonly used for lithology discrimination, thickness variation and sequences boundaries indicators associated with high contrasts in acoustic impedance values. It may also indicate unconformity surfaces, discontinuities, porosity and the presence of hydrocarbon in a reservoir (Oyeyemi, and Aizebeokhai, 2015; Alabi, and Enikanselu, 2019). The high relative acoustic impedance values are associated with shalier facies while lower values correspond to sand intervals. The high relative acoustic impedance may also be interpreted as sequences boundaries. Figure 14c shows the lowest relative acoustic impedance indicating reduced porosity and permeability due to hydrocarbon production.

Figure 15 represents the sweetness values of the seismic data. The sweetness value ranges from 0 (blue) to 22,500 (yellow). High sweetness values may be attributed to both high amplitude and low frequency while low sweetness value is as a result of low amplitude and high frequency in the seismic volume.

The high sweetness regions within the seismic data (circled in black) indicate high amplitude. They are interpreted as hydrocarbon-bearing sand units. Though the sweetness attribute is effective for channel detection and characterization of gas-charged bearing sand units, it is known to be less effective when the acoustic impedance

contrast between shale and sand units are low and when both lithology units are high. In most cases, shale intervals are characterized by low amplitude (low acoustic impedance contrasts) and high frequency thereby indicating low sweetness. Sand intervals are characterized by high amplitude (high acoustic impedance contrast with the shales) and low frequencies, thus indicating high sweetness values. Sweetness is used for identifying sweet spots that are hydrocarbon prone. The high sweetness values in the seismic section are possible indications of oil and gas (Okocha and Atakpo 2017). Figure 15c shows reduced high-amplitude areas due to hydrocarbon production (circled in black).

## 5. Conclusion and Future Recommendations

Production decline of 1192.21 bbl/day resulted from pressure decline of 95.50 bar/year or 0.062 psi/year. Most of the data points were not repeatable as evidenced in the computed Normalized root mean square (NRMS) of 0.38 meaning that on 62.0 % of Base and Monitor data points were coincident. A total of four sand bodies (L, M, N and O) were identified and correlated across all seven wells in the field. Two horizons (M and O) were selected for the study. Structural interpretation of seismic data revealed that the field is highly faulted with synthetic and antithetic faults which are in line with faults trends identified in the Niger Delta. Fault and horizon interpretation revealed that closures found are collapsed crestal structures bounded by two major faults. The depth structure maps reveal anticlinal faults. Reservoirs are found at a shallower depth from 10937 to 10997 ft and at a deeper depth ranging from 11681 to 11871 ft. The synthetic and antithetic faults act as good traps for the hydrocarbon accumulation in the study area. The variance edge and chaos enhanced the faults or sedimentological bodies within the seismic data volume. There are more discontinuities in the difference volume variance edge and chaos which show that there is production-induced fracturing in the field of study. The lengths, dips and orientations of the faults and horizons, in the base and monitor stacks, are not equal indicative of production-induced fault re-activation. The difference volume acoustic impedance shows the lowest relative acoustic impedance indicating reduced porosity and permeability due to hydrocarbon production while the difference volume sweetness shows reduced high-amplitude areas due to hydrocarbon production. In reservoirs, hydrocarbons were encountered by all seven wells drilled in the field. The following are some future suggestions (i) Studies should be done using geomechanical modeling to quantify the rate of reservoir compaction in a synthetic model for the formations in and around the depleting reservoirs. (ii) Fault seal analysis should be carried out to confirm that the suspected trapping faults are not leaking in which case they serve as conduits for hydrocarbon migrations rather than lateral barriers to hydrocarbon escape. (iii) Studies should be done on the mapping of thin sandstone reservoirs in the study area. (iv) Studies should be done using geomechanical modeling to quantify the stress changes in a synthetic model for the formations in and around the depleting reservoirs. (v) The estimated strains should be coupled to experimentally determine strain sensitivities to P-wave velocities of shale to predict time-shifts in the surroundings of the reservoirs.

### Declaration

### Source of Funding

This study did not receive any grant from funding agencies in the public, commercial, or not-for-profit sectors.

### Competing Interests Statement

The author declares no competing financial, professional, or personal interest.

#### **Consent for Publication**

The author declares that she consented to the publication of this study.

#### **Author's Contribution**

The author declares that she carried out the study.

#### **Informed Consent**

Not applicable.

#### **Availability of Data and Material**

The data and material used for this study was made available by Shell Petroleum Development Company of Nigeria (SPDC), Port Harcourt Nigeria.

#### **Institutional Review Board Statement**

Not applicable.

#### **Ethical Approval**

Not applicable.

#### **Acknowledgements**

The author is grateful to Shell Petroleum Development Company of Nigeria (SPDC), Port Harcourt Nigeria for the release of the academic data for the purpose of this study.

#### **Declaration of Artificial Intelligence**

The author declares that she did not use artificial intelligence during the course of this study.

#### **References**

- [1] Calvert, M.A., Cherrett, A.J., Micksch, U., Bourgeois, F.G., & Calvert, A.S. (2018). New time lapse seismic attribute linking 4D and geomechanics. In 80th EAGE Conference and Exhibition, Copenhagen, Denmark, Pages 15–12, SAGE.
- [2] Stammeijer, J.G.F., & Hatchell, P.J. (2014). Standards in 4D feasibility and interpretation. *The Leading Edge*, 33(2): 134–140.
- [3] Herwanger, J.V., & Koutsabeloulis, N. (2011). *Seismic geomechanics: How to build and calibrate geomechanical models using 3D and 4D seismic data*. EAGE Publications.
- [4] Landrø, M. (2001). Discrimination between pressure and fluid saturation changes from time-lapse seismic data. *Geophysics*, 66(3): 836–844.
- [5] Trani, M., Arts, R., Leeuwenburgh, O., & Brouwer, J. (2011). Estimation of changes in saturation and pressure from 4D seismic AVO and time-shift analysis. *Geophysics*, 76(2): 1–17.

- [6] MacBeth, C., Mangriotis, M.D., & Amini, H. (2019). Post-stack 4D seismic time-shifts: Interpretation and evaluation. *Geophysical Prospecting*, 67(1): 3–31.
- [7] Prioul, R., Bakulin, A., & Bakulin, V. (2004). Nonlinear rock physics model for estimation of 3D subsurface stress in anisotropic formations: Theory and laboratory verification. *Geophysics*, 69(2): 415–425.
- [8] Fuck, R.F., Tsvankin, I., & Bakulin, A. (2011). Influence of background heterogeneity on traveltimes shifts for compacting reservoirs. *Geophysical Prospecting*, 59(1): 78–89.
- [9] Ochoma, U. (2024). Seismic time-lapse effects of hydrocarbon production on the pressure, porosity and permeability regimes in FUBA Field, Onshore Niger Delta, Nigeria. *Irish Interdisciplinary Journal of Science & Research*, 8(1): 80–92.
- [10] Alsos, T., Eide, A., Astratti, D., Pickering, S., Benabentos, M., Dutta, N., Mallick, S., Schultz, G., Den B.L., Livingston, M., Nickel, M., Sonneland, L., Schlaf, J., Schoepfer, P., Sigimondi, M., Soldo, J.C., & Stronen, L.K. (2002). Seismic applications throughout the life of a reservoir. *Oilfield Review*, 14: 48–65.
- [11] Pourciau, R., Fisk, J., Descant, F., & Waltman, R. (2005). Completion and well performance results, Genesis Field, Deepwater Gulf of Mexico. *SPE Drilling and Completion*, 84415: 5–8.
- [12] Whiteman, A. (1982). Nigeria: Its petroleum geology, resources and potential. Graham and Trotman.
- [13] Adegoke, O.S., Oyebamiji, A.S., Edet, J.J., Osterloff, P.L., & Ulu, O.K. (2017). Cenozoic foraminifera and calcareous nannofossil biostratigraphy of the Niger Delta. Elsevier.
- [14] Short, K.C., & Stable, A.J. (1967). Outline of geology of Niger Delta. *Bulletin of the American Association of Petroleum Geologists*, 51(5): 761–779.
- [15] Horsfall, O.I., Uko, E.D., Tamunoberetonari, I., & Omubo-Pepple, V.B. (2017). Rock-physics and seismic-inversion based reservoir characterization of AKOS Field, Coastal Swamp Depobelt, Niger Delta, Nigeria. *IOSR Journal of Applied Geology and Geophysics*, 5(4): 59–67.
- [16] Ochoma, U. (2024). Petrophysical evaluation of FUBA Field reservoir in Onshore Niger Delta, Nigeria, using 3-D seismic and well logs. *Mediterranean Journal of Basic and Applied Sciences*, 8(1): 101–113.
- [17] Google (2018). Map of Niger Delta region showing the depo belts. Google Earth. Available at: <https://www.google.com/earth/>.
- [18] Aniwetalu, E.U., Anakwuba, E.K., Ilechukwu, J.N., & Aikegwonu, O.N. (2017). Application of time lapse (4D) seismic data in locating hydrocarbon prospects in Udam Field, Onshore Niger Delta, Nigeria. *Petroleum and Coal*, 59(5): 715–722.
- [19] Igwenagu, C.L., Uko, E.D., Tamunobereton-Ari, I., & Amakiri, A.R.C. (2021). The subsurface structures in KOCR Field in the Niger Delta, Nigeria, using 3D seismic timelapse data. *Geological Behavior*, 5(1): 7–12.
- [20] Ochoma, U. (2023). Hydrocarbon production induced faulting in Onshore FUBA Field, Niger Delta, Nigeria, using 3-D seismic time-lapse data. *Asian Journal of Applied Science and Technology*, 7(2): 185–196.

- [21] Ogbamikhumi, A., Tralagba, T., & Osagiede, E.E. (2017). Time-lapse seismic monitoring of offshore reservoirs in Niger Delta, Field ‘K’ as a case study. *Nigerian Journal of Environmental Sciences and Technology*, 1(1): 23–27.
- [22] Liang, S., Xu, Y., Shen, J., Wang, Q., Liang, X., Xu, S., Luo, C., Yang, M., & Ma, Y. (2025). Load–deformation behavior and risk zoning of shallow-buried gas pipelines in high-intensity longwall mining-induced subsidence zones. *Applied Sciences*, 15(19): 10618. <https://doi.org/10.3390/app151910618>.
- [23] Karanam, V., & Lu, Z. (2025). Poroelastic modeling and InSAR analysis of hydrocarbon production-induced surface deformation in the Permian Basin, USA. In *European Geosciences Union General Assembly 2025 (EGU25)*, Vienna, Austria. <https://doi.org/10.5194/egusphere-egu25-14878>.
- [24] Vedanti, N., Pathak, A., Srivastava, R.P., & Dimri, V.P. (2009). Time lapse (4D) seismic: Some case studies. *e-Journal Earth Science India*, 2(4): 230–248.
- [25] Varela, O.J., Torres-Verdin, C., Sen, M.K., & Roy, I.G. (2006). Using time-lapse seismic amplitude data to detect variations of pore pressure and fluid saturation due to oil displacement by water: A numerical study based on one-dimensional prestack inversion. *Journal of Geophysics and Engineering*, 3: 177–193.
- [26] Kragh, E., & Christie, P. (2002). Seismic repeatability, normalized RMS, and predictability. *The Leading Edge*, 21(7): 640–647.
- [27] Johnston, D.H. (2013). Practical applications of time-lapse seismic data. *SEG Distinguished Instructor Series No. 16*, SEG.
- [28] Schlumberger (2007a). *Interpreter’s guide to seismic attributes*.
- [29] Taner, M.T. (2001). Seismic attributes. *Canadian Society of Exploration Geophysicists Recorder*, 26: 48–56.
- [30] Law, W.K., & Chung, A.S.C. (2006). Minimal weighted local variance as edge detector for active contour models. In *Lecture Notes in Computer Science*, Pages 622–632, Springer.
- [31] Pigott, J.D., Kang, M.I.H., & Han, H.C. (2013). First order seismic attributes for elastic seismic facies interpretation: Examples from the East China Sea. *Journal of Asian Earth Sciences*, 66: 34–54.
- [32] Oyeyemi, K.D., & Aizebeokhai, A.P. (2015). Seismic attributes analysis for reservoir characterization: Offshore Niger Delta. *Petroleum and Coal*, 57(6): 619–628.
- [33] Alabi, A.A., & Enikanselu, P.A. (2019). Integrating seismic acoustic impedance inversion and attributes for reservoir analysis over ‘DJ’ Field, Niger Delta. *Journal of Petroleum Exploration and Production Technology*, 9: 2487–2496.
- [34] Okocha, F.O., & Atakpo, E. (2017). Effect of hydrocarbon production on reflection amplitude properties of reservoirs—A case of Kov Field, Niger Delta, Nigeria. *Arabian Journal of Geosciences*, 10(17): 380.